Fracture 1977, Volume 1, ICF4, Waterloo, Canada, June 19 - 24, 1977

SOME RECENT THEORETICAL AND EXPERIMENTAL DEVELOPMENTS IN FRACTURE MECHANICS

H. Liebowitz,* J. Eftis* and D. L. Jones*

ABSTRACT

Recent theoretical and experimental developments in four distinct areas of fracture mechanics research are described. These are as follows: experimental comparisons of different nonlinear fracture toughness measures, including the nonlinear energy, R curve, COD and J integral methods; the singular elastic crack-tip stress and displacement equations and the validity of the proposition of their general adequacy as indicated, for example, by the biaxially loaded infinite sheet with a flat crack; the thermodynamic nature of surface energy induced by propagating cracks in relation to a general continuum thermodynamic description of brittle fracture; and analytical and experimental aspects of Mode II fracture, with experimental data for certain aluminum, steel and titanium alloys.

INTRODUCTION

In this paper four different aspects of our research program in fracture mechanics are presented. They represent areas that involve problems that are yet to be resolved in a definitive manner, and areas that "break new ground," so to speak, certain to stimulate further research efforts in the future.

The first part concerns fracture toughness assessment for semi-brittle type fracture, i.e. beyond the linear elastic range. The second part challenges the general adequacy of the well-known "singular solution" for the elastic crack-tip stress and displacement components, illustrated through study of the biaxially loaded center-cracked sheet problem. The third part deals with crack propagation induced surface energy within the framework of a general continuum thermodynamic description of brittle fracture. The fourth part involves analytical and experimental aspects of Mode II fracture that indicate some results contrary to generally held opinions.

Because of space limitations some of the above mentioned areas will only be outlined, while in others only select parts will be discussed in detail sufficient to bring out the main ideas involved.

I. ASSESSMENT OF NONLINEAR FRACTURE TOUGHNESS

For semibrittle fractures, i.e. fracture under circumstances where crack front plastic yield may be too extensive to be ignored or treated as a minor correction and where fast fracture may be preceded by substantial subcritical crack growth, the problem of properly defining and evaluating

*School of Engineering and Applied Science, The George Washington University, Washington, D. C., U.S.A.

some measure of fracture toughness is currently a subject of controversy. Over the past 10-20 years several different measures have been proposed, the best known of which are, in order of chronological appearance, the R curve, COD, J integral and nonlinear energy methods.

The nonlinear energy method, first proposed by the authors several years ago [1,2], relies entirely on a statement of the global energy rate balance (First Law of Thermodynamics) appropriate to a fracture toughness test situation for its definition of fracture toughness. Let $\dot{W}$ and Q represent the global work rate of the applied forces and the rate of heat entering or leaving the cracked body, respectively. Further, let $\dot{E}$, $\dot{K}$ and $\dot{\Gamma}$ represent the rate of change of total energy of the body, with $\dot{E}$, $\dot{K}$ and $\dot{\Gamma}$, respectively, the rates of change of internal, kinetic and fracture energies. Then at each instant of crack propagation it is necessary that

$$\dot{W} + Q = \dot{E} + \dot{K} + \dot{\Gamma}, \tag{1}$$

where the dot represents time rate.

In a typical fracture toughness test situation, equation (1) may be simplified without serious loss of accuracy. It can be assumed that: (a) The test specimen during the conduct of the test is adiabatically isolated and everywhere isothermal, which requires that $Q \simeq 0$. If we assume the test specimen to behave elastoplastically, mechanically speaking, then under the thermal restraints imposed by condition (a), the global internal energy change is due entirely to changes in the elastic, U', and plastic, U'', energy of deformation,

$$E = U' + U'' . \tag{2}$$

(b) The test loading is usually slowly (quasi-statically) applied and, prior to onset of fast fracture, any crack extension that takes place will occur at a very slow rate. Hence, displacement rates will be small and the square of such rates will be smaller still, so that the kinetic energy rate can be approximately ignored, $\dot{K} \simeq 0$. Furthermore, due to the slow loading rate all changes in the field quantities such as stress, strain, displacement, etc., will be due to the changes in the quasi-statically applied load and/or the crack size. For a test specimen geometry with a through-the-thickness crack length, $c = 2a$, the time rate can be replaced by

$$\dot{} = \frac{\partial}{\partial t} = \dot{c}\,\frac{\partial}{\partial c} .$$

Thus during a test at each instant in which there is slow crack growth, under the conditions stated above, equation (1) can be reduced to

$$\frac{\partial W}{\partial c} = \left(\frac{\partial U'}{\partial c} + \frac{\partial U''}{\partial c}\right) + \frac{\partial \Gamma}{\partial c} . \tag{3}$$

Based on equation (3), the fracture toughness according to the nonlinear energy method [1,2] is written

$$\left[\frac{\partial W}{\partial c} - \left(\frac{\partial U'}{\partial c} + \frac{\partial U''}{\partial c}\right)\right]_{\substack{\text{onset}\\ \text{of fast}\\ \text{fracture}}} \equiv \tilde{G}_c . \tag{4}$$

It is noted that in this definition the fracture toughness represents the excess of the rate of work of the applied forces over the rate at which energy is absorbed in elastic and plastic deformation at the instant fast crack propagation ensues. No restrictions whatever have been placed on the possible extent of crack-front plastic yield (e.g., "small scale yield," "large scale yield," etc.) nor on the extent of subcritical crack growth. This definition is a natural generalization of that used in linear elastic fracture mechanics, and applies for both plane strain and nonplane strain conditions.

Since it is not possible at present to obtain an analytical (field derived) expression representing the left side of equation (4), other than by numerical means, an empirical method for measuring this quantity, based upon a single-test, load-displacement record, has been derived and successfully employed [cf. Figure 1]. The details of the derivation can be found in reference [2], and take the forms

$$\tilde{G}_c = \left\{ 1 + \frac{2nk}{n+1}\left[\frac{F_c}{M(c_0)}\right]^{n-1}\right\}\frac{1}{2B}F_c^2\,\frac{d}{dc}\left[\frac{1}{M(c_0)}\right] , \tag{5}$$

when there is no subcritical crack growth prior to fast fracture, and

$$G_c = \left\{ 1 + \frac{2nk}{n+1}\left[\frac{F_c}{M(c_c)}\right]^{n-1}\right\}\left(\frac{M(c_0)}{M(c_c)}\right)^2\frac{1}{2B}F_c^2\,\frac{d}{dc}\left[\frac{1}{M(c_0)}\right] , \tag{6}$$

when subcritical crack growth is present.

Experimental comparisons

In order to gain a better understanding of the empirical representations of the left side of equation (4), i.e., equations (5) and (6), a number of tests have been conducted and comparisons made between several other nonlinear fracture toughness parameters. Direct comparisons have been made between fracture toughness values obtained from the nonlinear energy method, $\tilde{G}_c$, J integral, J_{Ic}, COD method, G_{COD}, and the linear fracture toughness, $G_{Ic} = K_{Ic}^2/E$, for compact tension specimens of several alloys. Additional comparisons have been made between $\tilde{G}_c$ and G_R(R curve method) for thin center-cracked sheets of two aluminum alloys.

Since the selection of the critical point (the point at which the test data are used for fracture toughness assessment) represents the most important test variable, the rationale for its selection must be given careful consideration. The two most widely used critical points in nonlinear fracture toughness testing are: (a) the initiation of subcritical crack growth and, (b) the onset of unstable fracture (possibly including subcritical crack growth), which coincides with the maximum load for tests conducted in load control. Fracture toughness comparisons were made at both critical points so that the effect of subcritical crack growth on them could be revealed. The experimental procedures for evaluating each of the nonlinear fracture toughness parameters will be discussed briefly so that the basis for these comparisons will be understood.

Nonlinear energy method

The experimental procedure for evaluating equations (5) and (6) is quite straightforward due to the separation of the linear and nonlinear portions of $\tilde{G}_c$, that is, equation (5) may be written in the form

$$\tilde{G}_c = \tilde{C}\,\bar{G}_c \ ,$$

where

$$\bar{G}_c = \frac{1}{2B} P_c^2 \frac{d}{dc}\left[\frac{1}{M(c_0)}\right] \ ,$$

and equation (6)

$$\tilde{G}_c = \tilde{C}\left(\frac{M(c_0)}{M(c_c)}\right)^2 \cdot \bar{G}_c \ ,$$

where $\bar{G}_c$ is as shown above.

The linear portion, $\bar{G}_c$, can be obtained directly from standard expressions for the stress intensity factors and the appropriate G-K relations. It has been shown [3] that $\tilde{C}$ can be evaluated by the equation

$$\tilde{C} = 1 + \frac{2nk}{n+1}\left[\frac{F_c}{M(c)}\right]^{n-1} = 1 + \frac{2n(1-\alpha_2)}{\alpha_2(n+1)} \qquad (7)$$

where

$$n = 1 + \ln\left[\frac{\alpha_1(1-\alpha_2)}{\alpha_2(1-\alpha_1)}\right] \Big/ \ln\left(\frac{F_2}{F_1}\right) . \qquad (8)$$

In these equations the values of F_1 and F_2 are obtained from reduced-modulus secant lines drawn to the nonlinear load-displacement curve. The second secant line α_2 M, should intersect the load-displacement record at the critical point ($F_2 = F_c$) and the first should approximately bisect the angle between the tangent modulus, M, and α_2 M.

R curve

For the thin center-cracked panels tested, significant subcritical crack growth was observed so the fracture toughness according to the R curve method, G_R, was evaluated for comparison with the nonlinear energy fracture toughness. According to recent discussions on the R curve method [1,4], this fracture toughness measure is evaluated by substituting the crack size and load at the instability point into the appropriate linear relationship involving the stress intensity factor (regardless of the degree of crack front plastic yield). For the center-cracked sheet, the ASTM[5] polynomial relation was employed in the form

$$G_R = \frac{K_c^2}{E} = \frac{\sigma_c^2 \pi a_c}{E}\left[1 - 0.1\left(\frac{2a_c}{w}\right) + \left(\frac{2a_c}{w}\right)^2\right]^2 . \qquad (9)$$

As has been observed by many researchers, the determination of the critical crack size is difficult, especially for materials like the 2024-T3 aluminum in which the transformation from subcritical crack growth to unstable fracture appears to be a continuous process.

COD method

Although the concept involved in determining toughness values by the COD method is simple, its practical application is not a straightforward matter. It has been shown by a number of investigators that there is a relationship between the crack-tip opening, δ, and the linear fracture mechanics parameter G. For example Egan [6], based on a linear elastic analysis, shows this relation to be

$$\delta = \alpha \frac{G}{\sigma_{ys}} \ , \qquad (10)$$

where

$$\alpha = \begin{cases} 4/\pi \text{ for generalized plane stress conditions} \\ 4/\pi\sqrt{3} \text{ for plane strain conditions.} \end{cases}$$

It is now generally concluded [7] that because of the approximations involved in obtaining relation (10), α can be taken as having the value unity, and the toughness values evaluated from

$$G_{COD} = \sigma_{ys} \cdot \delta_c \qquad (11)$$

which is considered valid only at the onset of subcritical crack growth. In this expression δ_c represents the opening at the crack border, and is assumed to be a constant, characteristic of the material for a given thickness and temperature, regardless of the degree of plastic yield at the crack border, or of the specimen geometry and crack border strain field pattern. The principal experimental problem with the evaluation of G_{COD} lies in the precise determination of δ_c. Although a number of methods have been utilized by its proponents, the method used for these comparisons was to use a relation established by Egan [6] between the crack opening and clip gauge displacements.

J integral method

The J integral was originally defined as a path independent line integral in an elastic medium, linear or nonlinear [8]. However its evaluation as a plane strain nonlinear fracture toughness measure, J_{Ic}, that is, for elastic-plastic deformation, is based on an empirical measurement of the so-called "pseudo-potential energy" with crack size. This definition is actually the same as G_c for strictly linear elastic fracture, and $\tilde{G}_c$ for nonlinear fracture, provided there is no subcritical crack growth [2], because the J integral interpretation of the elastic-plastic problem is limited to a deformation theory of plasticity under conditions of monotonically increasing stresses at all points in the plastic region. For deeply notched bend-type specimens it has been shown [9] that J_{Ic} can be evaluated by the simple relation

$$J_{Ic} = \frac{2A}{Bb} \qquad (12)$$

where A is the area under the load-displacement record up to the critical point (i.e., either condition (a) or (b) above), and Bb is the remaining ligament. For these comparisons it was determined that the Ramberg-Osgood characterization of the load-displacement record could be integrated directly

to provide an expression for the area under the curve in the form

$$A = \frac{\tilde{C}F^2}{2M} \quad . \tag{13}$$

Results and discussion for center-cracked sheets

Although a number of fracture toughness tests have been conducted on center-cracked sheets of 7075-T6 and 2024-T3 aluminum alloys, the results of only one test series will be shown, since they are generally typical of the others. The results of the series of tests on 7075-T6 are shown in Figure 2. For these tests the standard center-cracked geometry without anti-buckling guides was used, and the displacements were measured at the load points. The specimen dimensions were w = 254mm, B = 1.6mm, c/w = 0.5, with gauge lengths varying between 178 and 813mm. Duplicate specimens were tested for each length and the results shown represent the average of each pair of tests. The tests were conducted in load control and subcritical crack growth was monitored visually with a hand-held magnifier (5-20X). As indicated in Figure 2, four fracture toughness values were obtained from each test. When the maximum load was utilized as the critical point, F_c and a_0 were used to evaluate $\tilde{G}_c$, while F_c and a_c were used to evaluate G_R. These values are seen in Figure 2 to possess considerable geometry dependence, with $\tilde{G}_c$ increasingly higher than G_R as the nonlinearity increased (decreasing gauge length). When the onset of subcritical crack growth was selected as the critical point, the original crack size and the load corresponding to a one percent increment of crack growth was used. This point was determined through direct measurement or by extrapolation of an R curve back to one percent crack growth. The lower two data points at each gauge length show the behavior of these toughness values.

These results demonstrate clearly that both $\tilde{G}_c$ and $\tilde{G}_R$ possess significant gauge length dependence, but that this dependence is due solely to the nonlinear response associated with subcritical crack growth. In addition, at the minimum length the nonlinear toughness $\tilde{G}_c$ is nearly twice $\tilde{G}_{sc}$ (evaluated at initiation of subcritical crack growth). This indicates the extent of the penalty imposed on the methods that do not incorporate subcritical crack growth into the fracture toughness assessment.

The $\tilde{G}_c$ values shown in Figure 2 were obtained by use of equation (5) which does not incorporate the subcritical crack growth directly into $\tilde{G}_c$. Therefore, the nonlinear energy method was again calculated to account more directly for the effects of subcritical crack growth in the manner indicated by equation (6). For certain of the center-cracked panels, $\tilde{G}_c$ was evaluated using both equations and the results were compared. It was found that the toughness values according to equation (6) averaged about seven percent higher than those from equation (5). Therefore, because of the considerably greater ease in evaluating equation (5), the data points shown in Figure 2 are based on this equation.

Results and discussion for compact tension tests

Additional comparisons, between the fracture toughness parameters $\tilde{G}_c$, J_{Ic}, G_{COD} and G_{Ic}, have been made from compact tension tests on several aluminum, titanium and steel alloys. For most of these materials, a series of tests were performed in which all dimensions of the specimen (w(width) = 76.2mm) were held constant except for the specimen thickness. In this manner the effect of increasing nonlinearity with decreasing thickness on the various toughness parameters could be determined and compared. As for

the center-cracked panels, the toughness values were evaluated for many of the test series at both the onset of subcritical crack growth and at unstable fracture. The two points were essentially coincident when the thickness was greater than $2.5(K_{Ic}/\sigma_{YS})^2$. For example, the results of the test series conducted on 2048-T851 aluminum in the L T orientation is shown in Figure 3. The values assumed by the four toughness measures when evaluated at the peak load are seen in Figure 3a. It is seen that all of the toughness parameters increased in a similar fashion as the thickness decreased below 36.1mm. The minimum thickness requirement for plane strain fracture for this material is greater than 25mm, while the proposed minimum value for constancy of J_{Ic}, $50\ J_{Ic}/\sigma_{YS}$, is less than 2.5mm. At maximum load the constancy of J_{Ic} as well as the other parameters is clearly not satisfactory. However, when the toughness values were evaluated at the onset of subcritical crack growth the results were quite different, as is seen in Figure 3b. Here it is seen that all of the toughness values with the possible exception of G_{COD} are quite independent of specimen thickness. Therefore, these results and the results from the center-cracked panels demonstrate that the subcritical crack growth causes most of the nonlinearities observed in fracture toughness testing, although it is recognized that crack-tip plasticity is necessary for subcritical crack growth to take place. The results of all of these comparisons suggest that if a realistic measure of fracture toughness is to be obtained for semibrittle fracture, it will be necessary to incorporate subcritical crack growth into the fracture toughness test methods.

Our fracture group is also currently engaged in a program whereby $\tilde{G}_c$ values are to be determined on the basis of finite-element calculations and compared with corresponding values obtained by our proposed test method of evaluation. This is being done initially for the case in which there is no substantial subcritical crack growth, with the hope of including the more general situation sometime in the near future.

II. ELASTIC CRACK-TIP STRESS, DISPLACEMENT, ENERGY RATE AND BIAXIALLY APPLIED LOADS.

It is more or less accepted in fracture mechanics that the elastic stress and displacement components very near to the tip of a plane line crack can be approximated with acceptable accuracy, for *all* plane cracked-body geometries and *every* in-plane outer boundary loading condition by a "one-parameter" or "one-term" representation, i.e. strictly in terms of the stress intensity factors K_I and/or K_{II}, e.g., equations (14), for the opening mode crack surface displacements

$$\begin{aligned}
\sigma_x &\simeq \frac{K_I}{(2\pi r)^{1/2}} \cos\frac{\theta}{2}\left(1 - \sin\frac{\theta}{2}\sin\frac{3\theta}{2}\right)\\
\sigma_y &\simeq \frac{K_I}{(2\pi r)^{1/2}} \cos\frac{\theta}{2}\left(1 + \sin\frac{\theta}{2}\sin\frac{3\theta}{2}\right)\\
\sigma_{xy} &\simeq \frac{K_I}{(2\pi r)^{1/2}} \sin\frac{\theta}{2}\cos\frac{\theta}{2}\cos\frac{3\theta}{2}\\
u_x &\simeq \frac{K_I}{\mu}\left(\frac{r}{2\pi}\right)^{1/2}\cos\frac{\theta}{2}\left(\frac{1}{2}(\kappa-1) + \sin^2\frac{\theta}{2}\right)\\
u_y &\simeq \frac{K_I}{\mu}\left(\frac{r}{2\pi}\right)^{1/2}\sin\frac{\theta}{2}\left(\frac{1}{2}(\kappa-1) - \cos^2\frac{\theta}{2}\right)
\end{aligned} \tag{14}$$

(cf. Figure 4), provided $0<r/a \ll 1$, where μ is the elastic shear modulus and κ is expressed in terms of Poissons' ratio $(3-4\nu)$ for plane strain and $(3-\nu)/(1+\nu)$ for idealized plane stress.

In a summary of our recent work which follows, it is shown that this practice, although literally time honored, is clearly unacceptable as a *general proposition* [10]. The reason lies with the quite arbitrary practice of disregarding the second term of the Williams' eigenfunction series representation for the plane stress components, a contribution which, relative to a rectangular (x-y) coordinate system, is independent of the radial distance from the crack tip. This practice can lead to serious error of both a quantitative and qualitative nature in the prediction of local stress, displacement and related quantities of interest, perhaps nowhere better illustrated than in the problem of the biaxially loaded sheet with a flat central crack (cf. Figure 4).

With the second term of the series expansion properly included, the stress and displacement components near the crack tip for the biaxial load problem take the form:

$$\sigma_x \simeq \frac{K_I}{(2\pi r)^{1/2}} \cos\frac{\theta}{2}\left(1 - \sin\frac{\theta}{2}\sin\frac{3\theta}{2}\right) -(1-\alpha)\,\sigma$$

$$\sigma_y \simeq \frac{K_I}{(2\pi r)^{1/2}} \cos\frac{\theta}{2}\left(1 + \sin\frac{\theta}{2}\sin\frac{3\theta}{2}\right)$$

$$\sigma_{xy} \simeq \frac{K_I}{(2\pi r)^{1/2}} \sin\frac{\theta}{2}\cos\frac{\theta}{2}\cos\frac{3\theta}{2} \qquad (15)$$

$$u_x \simeq \frac{K_I}{\mu}\left(\frac{r}{2\pi}\right)^{1/2}\cos\frac{\theta}{2}\left(\frac{1}{2}(\kappa-1) + \sin^2\frac{\theta}{2}\right) - \frac{(1-\alpha)(K+1)\sigma}{8\mu}\left(r\cos\theta + a\right)$$

$$u_y \simeq \frac{K_I}{\mu}\left(\frac{r}{2\pi}\right)^{1/2}\sin\frac{\theta}{2}\left(\frac{1}{2}(\kappa+1) - \cos^2\frac{\theta}{2}\right) + \frac{(1-\alpha)(3-K)\sigma}{8\mu}\,r\sin\theta.$$

provided $0<r/a \ll 1$ for the stress components and $0\leq r/a \ll 1$ for the displacement components.

The standard one-parameter characterization of the elastic crack-tip stress and displacement equations yield qualitatively as well as quantatively incorrect results for the local stresses and displacements. Note that for $u_x(r=0) = 0$ according to equation (14), which is obviously incorrect, whereas from equation (15),

$$u_x(r=0) = -\frac{(1-\alpha)\sigma\,(\kappa+1)a}{8\mu} \neq 0 \quad , \qquad (16)$$

as one would expect. Note also that equations (14) represent the proper approximations only for the case of equal biaxial tension-tension applied loads, i.e., $\alpha = 1$.

Equations (14) also yield incorrect results for the square of the maximum shear stress

$$\tau_m^{*2} \simeq \frac{\sigma^2\, a\, \sin^2\theta}{8r} \quad , \qquad (17)$$

compared to

$$\tau_m^2 \simeq \frac{\sigma\sqrt{\pi a}}{\sqrt{2\pi r}}\sin\frac{\theta}{2}\cos\frac{\theta}{2}\left(\frac{\sigma\sqrt{\pi a}}{\sqrt{2\pi r}}\sin\frac{\theta}{2}\cos\frac{\theta}{2} + (1-\alpha)\sigma\sin\frac{3\theta}{2}\right) + \frac{(1-\alpha)^2\,\sigma^2}{4} \quad , \qquad (18)$$

based on use of equations (15). Equation (18) can be rearranged to a form more convenient for the plotting of the maximum shear isostats, (cf. Figures 5,6a-6d)

$$\left[\left(\frac{\tau_m}{\sigma}\right)^2 - \left(\frac{1-\alpha}{2}\right)^2\right]\left(\frac{r}{a}\right) - \left[\frac{(1-\alpha)}{2\sqrt{2}}\sin\theta\sin\frac{3\theta}{2}\right]\left(\frac{r}{a}\right)^{1/2} - \frac{1}{8}\sin^2\theta = 0. \qquad (19)$$

As a result of the failure to include the second term of the stress series expansions, the substantial influence of the applied load biaxiality on these quantities is completely missed. Preliminary photoelastic experimental tests verify the predicted shift in the axis of the isostats between the equal tension-tension case, Figure 6b, and the uniaxial tension case, Figure 6c.

The same holds true with regard to prediction of the angle of initial crack extension. The maximum normal stress failure criterion was used as a basis for making these comparisons, although the *general* adequacy of this perhaps overly simple criterion is not necessarily endorsed. For lack of space, the mathematical analysis is omitted and only the important conclusions that follow from the use of equations (15) as against equations (14) are presented, (cf. Figures 7,8). Equations (14) always predict a zero angle of initial crack extension for *all* uniaxial-biaxial loading conditions, whereas equations (15) predict a turning of the angle of initial crack extension when the horizontal tensile load approaches about twice the vertical tensile load, increasing as the horizontal-to-vertical tensile load ratio increases. This result is in qualitative agreement with the tensile biaxial load experiments of Kibler and Roberts [11].

An important theoretical implication which follows as a consequence is the realization that one cannot, in general, assume a priori that a flat crack will always extend along its original plane under all symmetric in-plane loading conditions when making an Irwin G-K type calculation.

Omitting mathematical detail, the inclusion of the second terms of the series expansions for the stress and displacements, i.e., use of equations (15), can be shown to lead to the conclusion that the *local* elastic strain energy rate also has biaxial load dependency in the form

$$\frac{\partial U'}{\partial a} = G(r_0,\alpha) = \underbrace{A_1\,\sigma^2\,r_0}_{\text{I}} + \underbrace{A_2\,\sigma^2\,r_0\left(\frac{r}{a}_0\right)^{1/2}}_{\text{II}}(\alpha\text{-}1) \quad . \qquad (20)$$

In equation (20) U' is the total elastic strain energy over the local crack tip region, (cf. Figure 9), and A_1, A_2 are numerical coefficients of parts I and II, respectively, that include the elastic shear modulus and Poissons' ratio. Note that by use of equations (14) only the first term appears in equation (20). The second contribution to equation (20) cannot be dismissed as a "higher order effect," since for large values of α the second term can become appreciable relative to the first (cf. Table 1).

The result shown by equation (20) appears to be in conflict with the generally accepted understanding that the *global* elastic strain energy rate for the flat crack is completely independent of load biaxiality [12-14]. There appears here to be a contradiction, for how can the elastic strain energy rate depend *locally* on load biaxiality and yet appear to be independent of load biaxiality globally speaking?

An important practical consequence of these findings has to do with the possible dependence of plane strain fracture toughness, K_{Ic}, on biaxial loading. Further theoretical and experimental investigations of these questions are being considered by our research group.

III. SURFACE ENERGY AND ASPECTS OF THE CONTINUUM THERMODYNAMICS OF BRITTLE FRACTURE

Since the time of Griffith some fifty years ago, several seeming contradictions and paradoxes have persisted in fracture theory, which leave the foundations of the theory on tenuous and uncertain grounds. For example, consider the following fundamental questions: (a) The surface energy associated with the surfaces of a separating body, first introduced by Griffith, enter into fracture mechanics considerations through an addition of a surface energy rate term into the *global* energy rate balance (First Law of Thermodynamics). By virtue of this addition, however, the possibility of obtaining a corresponding *local* energy rate balance equation, as a derived consequence of the global balance statement, as is customary in the continuum mechanics for the nonseparating body, is lost. This fact either has not been recognized in fracture mechanics circles, or has been ignored until now. (b) Based on everyday experience, fracture should be thought of as an irreversible process. A body once cleaved in two will not spontaneously coalesce when, in otherwise identical circumstances, the sense of the applied loads which provoked the fracture is reversed. We know from nonequilibrium thermodynamics that irreversible processes must be associated with entropy production. Irreversible crack propagation should then, in some manner, contribute to the entropy of a separating body, and fracture should be viewed as a nonequilibrium (irreversible) continuum thermodynamic process. In circumstances which give rise to brittle fracture, elastic material response can be reliably assumed for the separating body, which, however, leads to a paradox. In thermally conducting elastic media, any entropy production occurs as a consequence of heat conduction. Furthermore, if the elastic media is ideally constrained to adiabatic or isothermal deformations, there is no entropy production at all. How then can the nonthermal part of the entropy content of a separating elastic body increase to agree with the requirement that crack propagation should

be responsible for increasing this quantity? (c) Surface energy plays an important part in the theoretical aspects of current fracture mechanics. Yet in the current theory the surface energy associated with a separating solid does not appear to be a clearly perceived and understood quantity. From the time of Griffith such surface energy has been generally regarded as a "material constant," with different physical interpretations, depending on who the investigator happens to be. However it is known experimentally that environmental effects clearly alter surface energy values. There also appears to be experimental evidence that for the self-propagating crack, surface energy is influenced by the crack propagation speed. Here experimental facts cannot support the "material constant" assumption for the surface energy induced on the surfaces of a propagating crack.

In a forthcoming paper, reference [15], a theory based on general continuum thermodynamics applied to a separating body, as well as on physical (atomic) considerations, appears to provide a rational explanation to the problems posed above. In our opinion the key to understanding these problems can be found by incorporating into general continuum balance laws the insight provided by physical theory [16,17], with regard to distributions of energy quantities on the material boundary surface of a solid, even though the densities of surface distributions will generally be some nine orders of magnitude smaller than corresponding volume distributions for solids of ordinary dimensions. For example it can be assumed that the total of any energy quantity, e.g., internal energy, free energy, entropy, etc., of any solid body consists of a volume contribution and a surface contribution, recognizing that for bodies of ordinary size, the surface contributions will be many orders of magnitude smaller than the volume contributions. If the surface is deformed and in a state of motion the same can also hold for surface mass density and momentum. In the continuum mechanics of the nonseparating body (which have *materially stationary* surfaces, even though the surfaces may be in a state of deformed motion) all surface energy distributions are tacitly ignored, and rightly so, in view of the very large order of magnitude differences.

For the separating body, however, (cf. Figure 10), while the surface energy distirubtions over the materially stationary surfaces $S_B = S_E + S_C$ can be ignored for the reasons mentioned above, the same cannot be said for newly created surfaces due to a propagating crack $S_F(t)$, which are materially nonstationary, that can grow very rapidly with time.

Because of space limitations we will show only the consequences of this point of view as it pertains to the total energy balance rate (First Law of Thermodynamics), and, to the entropy production rate (Second Law of Thermodynamics)* since these relate directly to the questions raised at the outset. A full discussion of the balance requirements for mass, linear momentum and moment of momentum, as well as a qualitative discussion of the underlying physical (atomic) aspects of surface energies and entropy on cut surfaces can be found in reference [15].

Let $\dot{W}$, Q, E and K represent, respectively, the work rate of the applied boundary tractions and body force, the rate at which heat is added or taken out of the body, the total internal energy and the total kinetic energy of the solid. Let ε, ψ, η represent volume densities (per unit mass) of the

*In this work the theory of nonequilibrium (irreversible) thermodynamics associated with the Truesdell-Coleman-Noll point of view [18,19] is followed. The reader is referred to reference [15] for a more complete discussion.

internal energy, the free energy and entropy, respectively, with ρ the mass density and θ the temperature. Furthermore, if ε^*, ψ^*, η^* and ρ^* represent the corresponding surface densities, because of the orders of magnitude difference between surface and volume densities, the relation between them can be symbolically written

$$| \zeta^* | << | \zeta | . \tag{21}$$

A dot appearing over a quantity represents the material or substantial time derivative

$$\dot{} = \frac{d}{dt}$$

since at this stage of discussion no restrictions of linearity of deformations (kinematic linearity) are made.

Assuming no form of interaction between the body and its surroundings other than through mechanical work and heat, then at each instant of crack propagation, the energy balance in the large requires that

$$\dot{W} + Q = \dot{E}[R] + \dot{K}[R] + \dot{E}[S_E + S_C] + \dot{K}[S_E + S_C] + \dot{E}[S_F(t)] + \dot{K}[S_F(t)] .$$

Because of condition (21) and the fact that $S_E + S_C$ are materially stationary surfaces, it follows that

$$\dot{E}[S_E + S_C] = \dot{K}[S_E + S_C] \equiv 0$$

as in the customary practice in the continuum mechanics of materially stationary (nonseparating) surfaces.

The postulated global energy rate balance for the separating solid, i.e. a body with a propagating crack is therefore

$$\dot{W} + Q = \dot{E}[R] + \dot{K}[R] + \dot{E}[S_F(t)] + \dot{K}[S_F(t)]. \tag{22}$$

It can be shown that equation (22) has the equivalent form (cf. reference [15])

$$\int_R \{\mathrm{tr}[\underset{\sim}{T}\underset{\sim}{D}] - \mathrm{div}\, \underset{\sim}{q} + \rho h - \rho\dot{\varepsilon}\}\, dV = \frac{d}{dt}\int_{S_F(t)} \rho^* \{\psi^* + \theta\eta^* + \tfrac{1}{2}\dot{\underset{\sim}{x}}\cdot\dot{\underset{\sim}{x}}\}\, dA \tag{23}$$

Here $\underset{\sim}{T}$ is the Cauchy stress tensor, $\underset{\sim}{D}$ is the rate of deformation tensor, $\underset{\sim}{q}$ is the heat conduction vector, ρh is the rate at which nonmechanical heat may be generated or lost internally per unit volume, $\underset{\sim}{x}$ is the position vector to any point of the body and $\dot{\underset{\sim}{x}}$ is the velocity, while tr stands for the trace operator. Note that although the integrand of the surface integral on the right side of (23) may be very small, the material time derivative over the fracturing surfaces $S_F(t)$ implicitly includes the quantity $\dot{A}_F(t)$, which is a measure of the crack propagation speed and which may be arbitrarily large.

As long as the crack propagates the right side of equation (23) cannot vanish, nor can it be converted to a volume integral over R through the

divergence theorem. Hence a direct derivation of a local form for energy rate balance from equation (23) is precluded.

It is emphasized that as a consequence of the introduction of surface quantities into the thermodynamic description of the fracture process, a major departure from the mechanics appropriate to a nonseparating body becomes necessary. All local equations for rate of balance (except the one for mass) are no longer obtainable as derived consequences of the postulated global rate of balance equations, as is usual for classical continuum mechanics, i.e., for nonseparating bodies. In the case of crack propagation they must instead be introduced as separate additional postulates alongside the global postulates. For a full discussion of this question the reader is referred to reference [15].

Using the arguments given in reference [15], the local energy rate balance must be introduced as a separate postulate in the form

$$\mathrm{tr}[\underset{\sim}{T}\underset{\sim}{D}] - \mathrm{div}\, \underset{\sim}{q} + \rho h - \rho\dot{\varepsilon} = 0. \tag{24}$$

In the conventional point of view with regard to the global energy balance in fracture mechanics, it is customary to write in terms of the notation employed here

$$\dot{W} + Q = \dot{E}[R] + \dot{K}[R] + \dot{\Gamma} . \tag{25}$$

The energy rate term $\dot{\Gamma}$ is interpreted by some as a form of "energy dissipation" associated with the crack propagation, and is assumed, following Griffith, to be proportional to the fractured surface area [20]

$$\dot{\Gamma} = \frac{d}{dt}\int_{S_F(t)} \gamma_0\, dA = \gamma_0\, \dot{A}_F(t) . \tag{26}$$

The proportionality factor γ_0 is assumed to be a constant of the material, variously referred to as the "specific fracture surface energy," and "true surface energy," the "apparent surface energy," or sometimes even as the "surface tension" of the solid, with physical interpretations that are correspondingly varied. Perhaps the most common interpretation holds that γ_0 represents the energy necessary to form a unit area of new surface. Of course by placing $\dot{\Gamma}$ to the right side of equation (25) it is acknowledged thereby that crack propagation alters the total energy content of the body. However, specification of $\dot{\Gamma}$ by means of equation (26) simply assigns a constant surface energy density to the newly formed fractured surfaces with no rationale for such a choice, thereby leaving the meaning of γ_0 somewhat vague. It is also noted that, with the addition of $\dot{\Gamma}$ as defined by equation (26) to the right side of equation (25), the local energy rate balance (24) can never be obtained as a derived consequence. To the best of the authors' knowledge this fact has never been discussed in the literature.

The surface energy rate terms in either equations (22) or (23) are obvious generalizations of the $\dot{\Gamma}$ contribution to equation (25). It would appear therefore that a general and rationally based definition of $\dot{\Gamma}$ appropriate to the consideration of crack propagation as a thermodynamic process should be

$$\dot{\Gamma}[S_F(t)] \equiv \dot{E}[S_F(t)] + \dot{K}[S_F(t)] = \frac{d}{dt}\int_{S_F(t)} \gamma^*(\underset{\sim}{x},t)\, dA , \tag{27}$$

where $\gamma^*(\underset{\sim}{x},t)$ is the thermodynamic surface energy density associated with the fractured surfaces, i.e.

$$\gamma^* \equiv \rho^* \{\psi^* + \theta\eta^* + \frac{1}{2}\,\dot{\underset{\sim}{x}}\cdot\dot{\underset{\sim}{x}}\} \quad \text{on } S_F(t) \ . \tag{28}$$

In general, it is seen that the surface energy density induced on the surfaces of a propagating crack consists physically of the energy due to the deformation of the fractured surfaces through ψ^*, the heat in such surfaces through $\theta\eta^*$, and the kinetic energy due to the motion of the separating surfaces, $1/2\ \dot{\underset{\sim}{x}}\cdot\dot{\underset{\sim}{x}}$. The energy induced on the surfaces of a propagating crack, from a general thermodynamic point of view, is therefore seen to be quite complicated, and certainly is in no way a general "material constant."

The global condition for irreversibility, the so-called Second Law of Thermodynamics, generalized to nonhomogeneous thermodynamic processes and modified to include the surface entropy induced by the crack propagation, requires that the rate of entropy production be nonnegative, or

$$\dot{P} = \dot{P}[R] + \dot{P}[S_F(t)] = \int_R \rho\dot{\eta}\ dV + \frac{d}{dt}\int_{S_F(t)} \rho^*\eta\ dA - \int_{S(t)} \{-\frac{1}{\theta}\,\underset{\sim}{q}\cdot\underset{\sim}{n}\}\ dA$$
$$- \int_R \frac{1}{\theta}\ h dV \geq 0 \ . \tag{29}$$

$\dot{P}$ is the global entropy production rate and $\underset{\sim}{n}$ is an an outwardly directed unit normal vector to the surface S(t). Implied here is the condition that the entropy production rate over the materially stationary surfaces is negligible: $\dot{P}[S_E + S_C] \equiv 0$. Equation (29) can be equivalently represented in the form

$$\dot{P} = \int_R \{\rho\dot{\eta} + \mathrm{div}[\frac{1}{\theta}\,\underset{\sim}{q}] - \frac{1}{\theta}\,\rho h\} dV + \frac{d}{dt}\int_{S_F(t)} \rho^*\eta^*\ dA \geq 0 \ . \tag{30}$$

Again, while the crack propagates the surface integral cannot vanish, which again means that a local condition for irreversibility cannot be derived directly from the global postulate (30). Employing the same reasoning which led to equation (24) (cf. reference [15]), a local form for the entropy production of a separating body must be additionally postulated in the form

$$\rho\dot{\eta} + \frac{1}{\theta}\ \mathrm{div}\ \underset{\sim}{q} - \frac{1}{\theta^2}\underset{\sim}{q}\cdot\mathrm{grad}\ \theta - \frac{1}{\theta}\,\rho h \geq 0 \ . \tag{31}$$

An important characteristic for a separating body can be immediately deduced from equation (30). For crack propagation that is induced by an isentropic deformation in which the body is also adiabatically isolated, $\dot{\eta} = h = 0$ in R, $\underset{\sim}{q} = 0$ on S(t); it follows from equations (29) and (30) that

$$\dot{P} = \frac{d}{dt}\int_{S_F(t)} \rho^*\eta^*\ dA \geq 0 \ . \tag{32}$$

In other words, crack propagation in an adiabatically isolated body can never decrease the total entropy of a separating body.

In the limited space available several further important consequences of the general theory are summarized. Assuming a purely mechanical theory of brittle (linear elastic) fracture, the thermodynamic variables temperature and entropy remain at fixed uniform reference values θ_0, η_0, as does

the mass density ρ_0. In the absence of a temperature gradient, heat conduction vanishes and no internal source of heat generation or loss is assumed. Since $q_k = \rho_0 h = 0$ at each point in R, it follows that the body is adiabatically isolated. The volume free energy in a small deformation theory, when expanded as a Taylor series about the undeformed reference state can be shown to have the form (cf. reference [15]), referred to a fixed rectangular coordinate system x_k, k = 1,2,3,

$$\rho_0\ \psi(e_{jk},\ \theta_0) \simeq \rho_0\ \psi_0(0,\ \theta_0) + \frac{1}{2}\ C_{jklm}\ e_{jk}\ e_{lm}, \tag{33}$$

where e_{jk} are the components of the linearized strain tensor and C_{jklm} are the second-order elastic coefficients. In strong solids restricted to small displacement gradients, the positive-definite quadratic form

$$\frac{1}{2}\ C_{jklm}\ e_{jk}\ e_{lm} \equiv \phi(e_{rs}) \tag{34}$$

defines the elastic strain energy density of the deformed state, so that the volume free energy can be written equivalently as

$$\rho_0\ \Psi(e_{jk},\ \theta_0) = \rho_0\ \psi_0(0,\theta_0) + \phi(e_{jk}) \ . \tag{35}$$

The first term on the right side of equation (35) represents the free energy in the undeformed reference state, and is a measure of the intrinsic binding energy of the solid at the reference temperature, θ_0. The linear elastic constitutive equations have the well known form

$$t_{jk} = \frac{\partial\phi}{\partial e_{jk}}\ (e_{rs}) = C_{jklm}\ e_{lm} \ , \tag{36}$$

where t_{jk} are the components of the Cauchy stress tensor.

With fixed thermal conditions the volume internal energy is easily shown to be due entirely to the rate of change of the elastic strain energy.

$$\dot{E}[R] = \int_R \rho_0\ \dot{\varepsilon}\ dV = \int_R \dot{\phi}(e_{jk})\ dV = \int_R t_{jk}\ \dot{e}_{jk}\ dV = \dot{\Phi}[R] \ . \tag{37}$$

In the absence of thermal effects in an idealized linear theory the global energy rate balance (22) appropriate to brittle crack propagation reduces to

$$\dot{W} = \dot{\Phi}[R] + \dot{K}[R] + \frac{d}{dt}\int_{S_F(t)} \gamma^*(x_i,t)\ dA \ . \tag{38}$$

Correspondingly the general thermodynamic surface energy density (28) induced on the fractured surfaces reduces to the form

$$\gamma^* = \rho_0^*[\psi_0^*(0,\theta_0) + \phi^*(e_{jk}) + \theta_0\eta^* + \frac{1}{2}\,\dot{u}_k\,\dot{u}_k] \quad \text{on } S_F(t) \ , \tag{39}$$

where u_k are the components of the displacement vector. The surface energy on the fractured surfaces thus consists of four contributions, respectively:

the surface free energy at the reference state, due essentially to the planar cohesive energy of the material surface; the surface strain energy density due to the deformation of the fractured surfaces; the latent heat in these surfaces; and the kinetic energy due to their motion.

For the self-propagating crack, i.e. for crack propagation under ideally "fixed-grip" conditions with body force neglected, the time rate of change of all field quantities can now only be attributed to the changing crack size $A_F(t)$. Thus in a linearized theory under "fixed-grip" conditions

$$\dot{} = \frac{\partial}{\partial t} = \dot{A}_F \frac{\partial}{\partial A_F} \quad .$$

Accordingly the general balance equation (38) takes the form

$$-\frac{\partial \Phi}{\partial A_F} = \frac{1}{2}\rho_0 \frac{\partial}{\partial A_F}\left[\dot{A}_F^2 \int_R \left(\frac{\partial u_k}{\partial A_F}\cdot\frac{\partial u_k}{\partial A_F}\right) dV\right] + \frac{\partial}{\partial A_F}\int_{S_F(t)} \gamma^*(x_i,t)\, dA, \tag{40}$$

while (39) becomes

$$\gamma^* = \rho_0[\psi_0^*(0,\theta_0) + \phi^*(e_{jk}) + \theta_0\eta^* + \frac{1}{2}\left(\frac{\partial u_k}{\partial A_F}\cdot\frac{\partial u_k}{\partial A_F}\right)\dot{A}_F^2] \quad . \tag{41}$$

Equation (40) is a nonlinear equation in $A_F(t)$ which serves as the governing equation for the crack propagation speed. It has in fact been used by Mott and Roberts and Wells (with several rather drastic simplifying approximations) as the starting point for an estimate of the terminal speed of the self-propagating crack running at constant velocity in brittle fracture. Equation (41) demonstrates explicitly the nonlinear crack speed dependency of the surface energy for the self-propagating crack, recently observed experimentally [21-23].

Let γ_S^* designate the surface energy for a slowly expanding crack, as in subcritical crack growth, $(\dot{u}_k\ \dot{u}_k) \ll 1$ on $S_F(t)$. Then clearly

$$\gamma_S^* < \gamma^* \quad . \tag{42}$$

The surface energy induced by subcritical crack growth is always less than the surface energy associated with a fast propagating crack.

Finally it is noted that the ratio

$$\frac{\gamma^*}{\gamma_S^*} = 1 + \left[\frac{1}{2}\frac{\rho_0^*}{\gamma_S^*}\left(\frac{\partial u_k}{\partial A_F}\cdot\frac{\partial u_k}{\partial A_F}\right)\dot{A}_F^2\right] \leq D \tag{43}$$

must have an upper bound for self-propagating cracks since experiments show that the crack speed $\dot{A}_F$ has a maximum speed of the order of one-half the elastic shear wave propagation speed. Inequality (43) disagrees in one respect with the results reported in reference [22], taken from the experimental data of reference [21], in which the ratio γ^*/γ_S^*, although increasing nonlinearly with crack speed, approaches infinity at the terminal crack speed, a result which, physically speaking, is highly unlikely to occur.

IV. MODE II FRACTURE

The edge-sliding mode of fracture (Mode II) was defined and analyzed a number of years ago. However, practical examination of Mode II fracture has been essentially ignored until recently. The lack of interest was apparently due to the belief that the K_{IIc} toughness values are so much higher than K_{Ic} values for a given material that, as a consequence, isotropic materials will not fail in Mode II. However, Jones and Chisholm [24] have recently shown that this is not the case for 2024-T4 aluminum plate, as well as for a number of other important structural materials [25]. This research was primarily motivated by the present lack of knowledge about Mode II fracture and by some observations of Mode II fracture initiation in frangible bases of highway luminaire supports.

Analysis

In order to develop an understanding of Mode II fracture, the compact shear (CS) specimen shown in Figure (11) was conceived and then analyzed by boundary collocation techniques using the complete, asymmetric Williams stress function [25,26]. Due to the symmetry of the CS specimen about its centerline, it was necessary to analyze only one-half of the specimen. The analytical method was based on requiring Williams' [27] eignefunction expansion of a stress function, χ, to satisfy the boundary conditions at a finite number of points around the specimen boundary. Also, since the specimen was asymmetric about the crack tips, it was necessary to employ the complete Williams stress function (symmetric and antisymmetric parts) in the collocation analysis. The stresses and stress intensity factors were obtained as a function of χ and it was determined that the Mode II stress intensity factor was given by

$$K_{II} = \sqrt{2\pi}\ B_{4,1} \quad , \tag{44}$$

where $B_{4,1}$ is the first odd coefficient of the series expansion for χ (the coefficient of the antisymmetric $r^{-1/2}$ term for the stresses).

Since only one-half of the specimen was analyzed it was necessary to determine the distribution of normal stresses along the centerline, E-F (cf. Figure 11). Both linear and bilinear normal stress distributions were assumed in the stress analysis [28] and a subsequent oblique incidence photoelastic experiment was employed to determine the actual stress distribution. The photoelastic experiment verified that the bilinear stress distribution provided the best first-order representation of the centerline stresses.

The boundary collocation method was solved numerically on an IBM 360-65 computer and good convergence was obtained when the computer program collocated on the stress function and its normal derivative. The program was then exercised to determine the effects of variations in specimen geometry on the Mode II stress intensity factor and, thus, to optimize the specimen geometry.

Since no prior analysis of the CS specimen existed, it was decided that a photoelastic analysis should be conducted to verify the Mode II crack-tip stress distribution and the stress intensity factors. To accomplish this a CS specimen was fabricated from Hysol resin 4290-CP5 with the dimensions, w = 95.0mm, H = 24.4mm and B = 7.14mm. A conventional transmission photoelastic experiment was performed in which both light and dark field results were recorded [28]. The photoelastic analysis verified that

the desired Mode II stress distribution existed at the crack tip. Also, the Mode II stress intensity factors obtained from the photoelastic results agreed quite well with the boundary collocation results as seen in Figure 12. The stress intensity factors obtained from the boundary collocation program are given in Figure 12 as a function of a/w for linear and bilinear normal centerline distributions. It was concluded from these results that the stress intensity factor could be given by

$$K_{II} = \sigma\, a^{1/2},\quad 0.3 < a/w < 0.7 \tag{45}$$

and

$$K_{II} = 1.08\sigma\, a^{1/2},\quad a/w = 0.8 \tag{46}$$

to within an accuracy of two percent. Of course, these particular values of the stress intensity are only valid for the dimensions of the photoelastic specimen.

Testing and results

After the analysis of the CS specimen was completed, an experimental research effort was initiated to obtain some knowledge about the Mode II fracture characteristics of several aluminum, titanium and steel alloys. Two specimen geometries, which differed slightly from the photoelastic specimen, were employed using H = 28.6mm and w = 63.5 or 76.2mm. The smaller w values were selected for the purpose of reducing the fracture load. A set of Mode II fracture mechanics grips was designed and fabricated so that the displacements could be measured using a standard fracture mechanics clip gauge. The experimental procedure was designed to follow as closely as possible the Mode I fracture toughness test specifications established in ASTM E399. For example, the five percent secant offset load was used in the appropriate formulas for the stress intensity factor.

The primary objectives of this testing program were: (a) to examine the characteristics associated with fracture in the edge-sliding mode, (b) to ascertain the effects of specimen geometry on Mode II fracture, and (c) to establish geometry-independent K_{IIc} values for various structural materials. The first objective was of considerable interest because of the viewpoint held by many researchers that isotropic structural materials will not fail in the maximum shear direction. However, all of the medium and high toughness materials that were examined as part of this testing program failed in unstable fracture along, or close to the plane of maximum in-plane shearing stress (along the plane of the initial crack). In most cases the direction of crack growth diverged less than five degrees from the plane of maximum shear. The fracture surfaces on these specimens were much flatter and brighter than the Mode I fracture surfaces for the same material. Both features were determined by subsequent examination to have been caused by the abrading action of one fracture surface against the other resulting from the parallel displacements associated with the edge-sliding mode. Many of the fracture surfaces have been examined by optical and scanning electron microscopy. It was concluded that the primary failure mechanism was shear microvoid coalescence and also that most of the surface abrasions were created during unstable crack propagation, rather than during crack initiation [29]. A photograph of a typical Mode II fracture surface is seen in Figure 13.

The second objective-determination of the effects of specimen geometry on Mode II fracture-has only been examined in a limited manner. It has been observed that crack tip radii below 0.13mm, a/w ratios, and specimen thickness apparently have limited effect on the K_{IIc} values. However, only the specimen thickness was examined in a systematic manner for several structural materials. Thus at this time it is reasonable to conclude only that these variables in the ranges examined do not significantly influence the Mode II fracture toughness values.

An example of the satisfaction of the third objective is presented in Table 2, which gives K_{IIc} values for only a few of the tests that have been performed. The subscript c was used for these toughness values even though no validity criteria have been established for Mode II testing. The K_{Ic} values were also included in Table 2 for comparison purposes. It is noted first that the K_{IIc} values were approximately twice as large as the K_{Ic} values for the 7075-T651 and 2124-T851 aluminum alloys. However, specimens from both alloys failed in the Mode II direction and fractured in an unstable manner after a limited amount of subcritical crack growth.

For the A533-B steel it is seen that the K_{IIc} values are much lower than estimated K_{Ic} values (no valid K_{Ic} tests have been conducted at room temperature because of the very large thickness requirements). However, extensive crack-tip plasticity was observed prior to unstable fracture in these tests so it is doubtful whether linear fracture criteria could be properly applied to Mode II tests on this material.

The results of the tests on Ti-6Al-4V in the β forged condition are typical of the one shown in Table 2 and indicate that K_{IIc} values were generally 15-20 percent below the corresponding K_{Ic} values. The tests on the titanium alloy resulted in very limited plasticity so that it is probable that they can be properly treated by linear fracture techniques.

As a result of these tests and others [25] it has been concluded that Mode II fracture can represent a practical fracture mode when structural loads are applied in the Mode II direction. It also appears that for certain alloys unstable fracture can occur in the edge-sliding Mode at lower stress intensity values than in the opening mode. In addition, Mode II fracture also appears to represent a very significant technological problem for anistropic and composite materials.

ACKNOWLEDGEMENTS

The authors wish to acknowledge partial financial support from the NASA-Langley Research Center thru Grant NGR 09-010-053, and the Office of Naval Research thru Contract No. NR064-Navy-0014-67-A-0214-0018.

REFERENCES

1. EFTIS, J. and LIEBOWITZ, H., Engr. Fract. Mech., 7, 1975, 101.
2. EFTIS, J., JONES, D. L. and LIEBOWITZ, H., Engr. Fract. Mech., 7, 1975, 491.
3. JONES, D. L., LIEBOWITZ, H. and EFTIS, J., Engr. Fract. Mech., 6, 1974, 639.
4. Fracture Toughness Evaluation by R Curve Methods. ASTM STP 527, Am. Soc. Test. Matl's., Philadelphia, 1973.

5. BROWN, W. J. and SRAWLEY, J. E., Plane Strain Crack Toughness Testing of High Strength Metallic Materials, ASTM STP 410, Am. Soc. Test. Matl's., Philadelphia, 1969.
6. EGAN, G. R., Engr. Fract. Mech., 5, 1973, 167.
7. SUMPTER, J. D. G. and TURNER, C. E., Second International Conference on Pressure Vessel Technology, 1973.
8. RICE, J. R., Fracture, Vol. 2, (ed. Liebowtiz, H.), Academic Press, New York, 1968, 191.
9. LANDES, J. D. and BEGLEY, J. A., Scientific Paper 73-1E7-FMPWR-P3, Westinghouse Research Lab., 1973.
10. EFTIS, J., SUBRAMONIAN, N. and LIEBOWITZ, H., Engr. Fract. Mech., forthcoming, 1976.
11. KIBLER, J. J. and ROBERTS, R. J., Eng. for Industry, Trans. ASME, 1970, 727.
12. GRIFFITH, A. A., Proc. First Int. Congress Appl. Mech., Delft, 1924, 55.
13. MOSSAKOVSKII, and RYBKA, M. T., PMM, 29, 1965, 291.
14. SIH, G. C. and LIEBOWITZ, H., Int. J. Solids Structures, 3, 1967, 1.
15. EFTIS, J. and LIEBOWITZ, H., Engr. Fract. Mech., forthcoming, 1976.
16. HERRING, C., Structures and Properties of Solid Surfaces, (eds. Gomer, R. and Smith, C.), Univ. Chicago Press, 1953, 1.
17. Surface Physics of Materials, Vols. 1,2 (ed. Blakely, J.), Academic Press, New York, 1975.
18. TRUESDELL, C., Modern Developments in the Mechanics of Continua, (ed. Eskinazi), Academic Press, New York, 1966.
19. TRUESDELL, C. and NOLL, W., Encylopedia of Physics, (ed. Fluge, S.) Vol. III/3, Springer, New York, 1965.
20. ERDOGAN, F., Fracture, Vol. 2, (ed. Liebowitz, H.) Academic Press, New York, 1968, 497.
21. PAXSON, T. L. and LUCAS, R. A., Int. Conf. Dynamic Crack Propagation (ed. Sih, G. C.), Noordhoff, Leyden, 1973, 415.
22. BERGKIRST, H., J. Mech. Phys. Solids, 21, 1973.
23. NILSSON, F., Engr. Fract. Mech., 6, 1974.
24. JONES, D. L. and CHISHOLM, D. B., Engr. Fract. Mech., 7, 1975, 261.
25. CHISHOLM, D. B., D.Sc. Dissertation, The George Washington University, Washington, D. C., 1975.
26. CHISHOLM, D. B., Progress Reports Nos. 4 and 5, Federal Highway Administration, Washington, D. C., 1973.
27. WILLIAMS, M. L., Trans. Am. Soc. Mech. Engrs., 79, 1957, 100.
28. CHISHOLM, D. B. and JONES, D. L., Exptl. Mech., forthcoming, 1976.
29. JONES, D. L. and CHISHOLM, D. B., Fractography - Microscopic Cracking Processes, ASTM STP 600, Am. Soc. Test. Matl's., Philadelphia, forthcoming, 1976.

Table 1. Error Involved by Use of Equations (14) to Obtain Equation (20)

Biaxial Load Factor α	0	1	2	3	-1	-2	-3
% $\frac{II}{I}$	$-3^{1/2}$	0	$3^{1/2}$	7	-7	-11	-14

Table 2. Comparison of Mode I and II Fracture Toughness Values for Several Structural Materials

Material	Thickness (mm)	a/w Ratio	K_{IIc} MPa$\sqrt{m}$	K_{Ic} MPa$\sqrt{m}$
7075-T651	9.55	0.548	56	26
2124-T851	6.35	0.547	59	30
A533-B	6.35	0.697	69	132-220*
Ti-6A -4V	9.53	0.700	74	88

*Estimated range of values

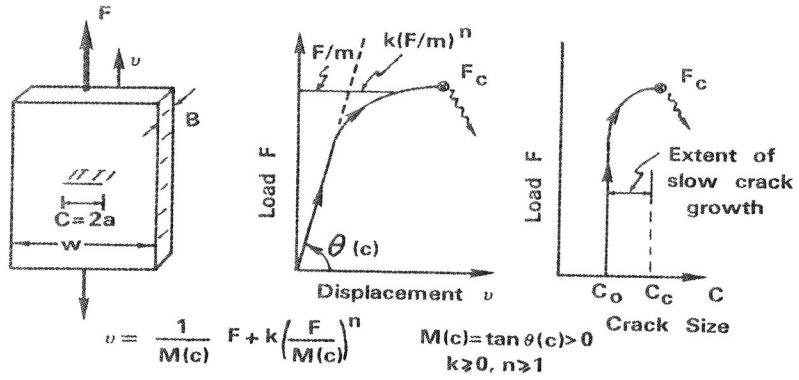

Figure 1 Typical fracture mechanics test results showing crack-tip plasticity and subcritical crack growth

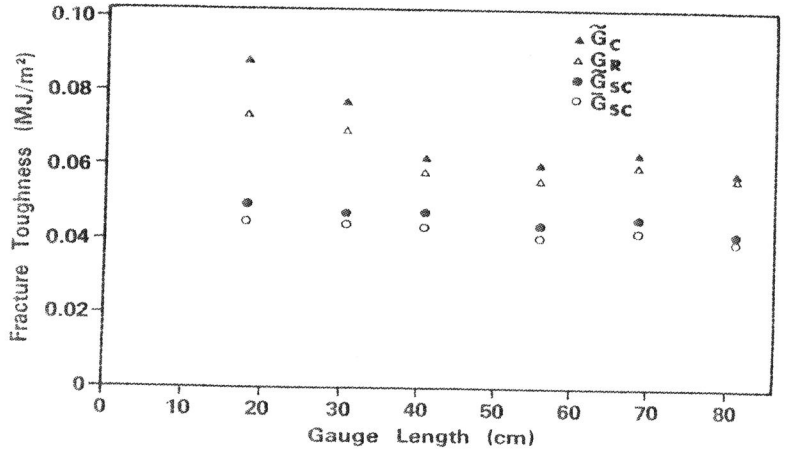

Figure 2 Fracture toughness of 7075-T6 sheets as a function of gauge length, evaluated at the onset of sub-critical crack growth and at peak load

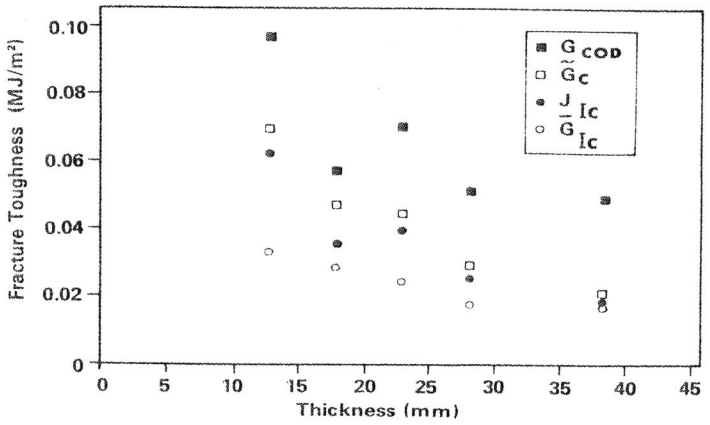

Figure 3a Variation of toughness parameters with specimen thickness for 2048-T851 (L-T) determined at peak load (incorporating subcritical crack growth)

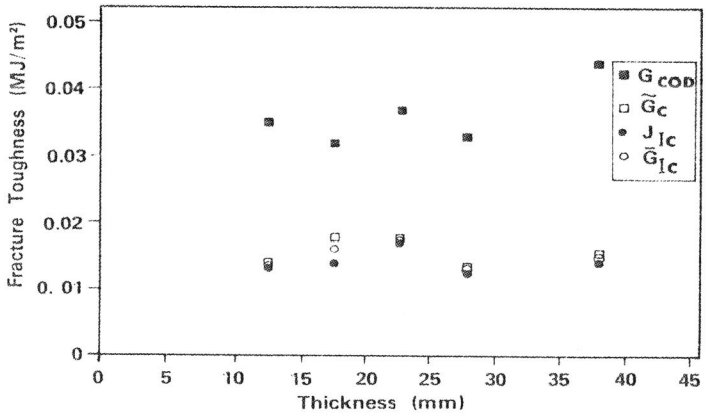

Figure 3b Variation of toughness parameters with specimen thickness for 2048-T851 (L-T) determined at the onset of subcritical crack growth

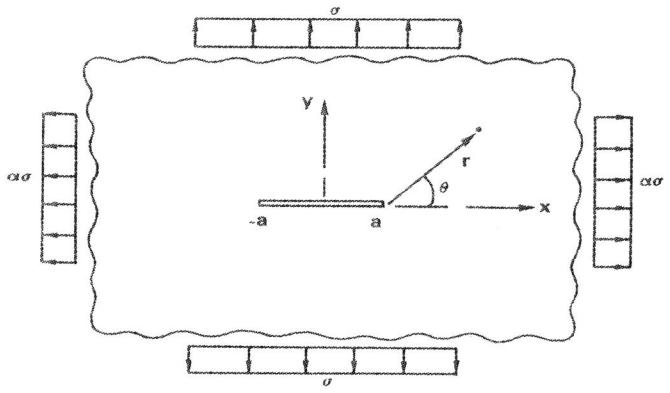

Figure 4 Plane biaxially loaded center-cracked geometry

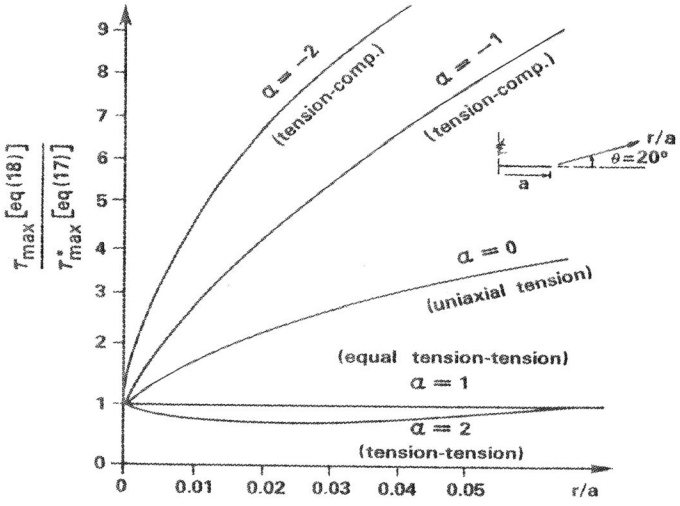

Figure 5 Error in the conventional shear stress calculation near the crack tip, for $\theta = 20^0$

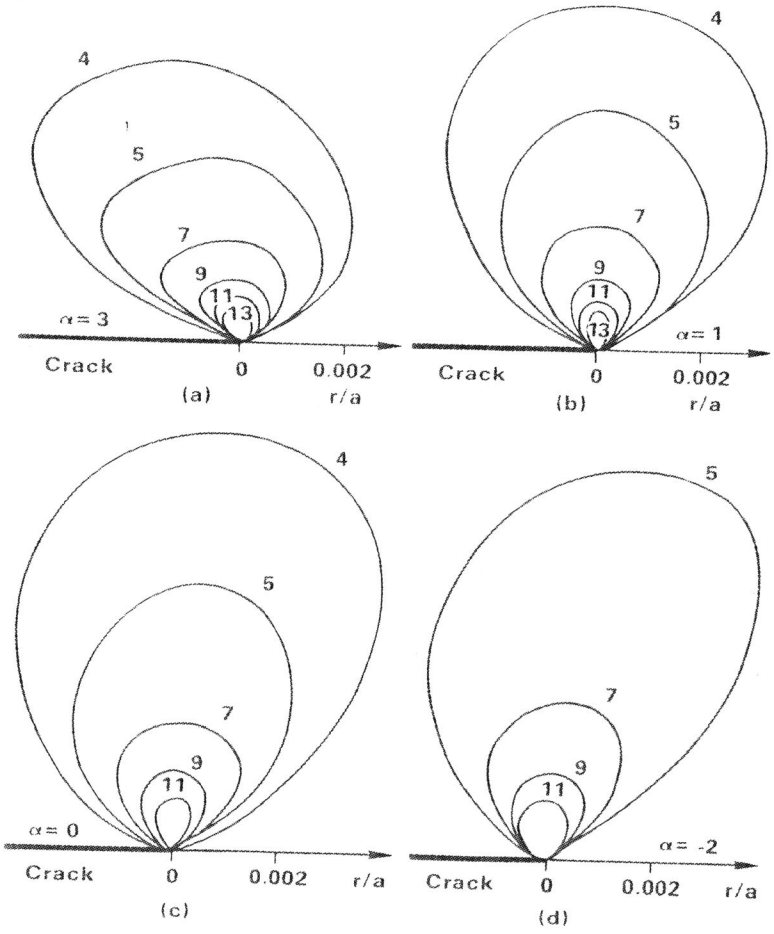

Figure 6 Contours of constant shear stress as a function of the load biaxiality: (a) $\alpha = 3$, (b) $\alpha = 1$, (c) $\alpha = 0$, and (d) $\alpha = -2$.

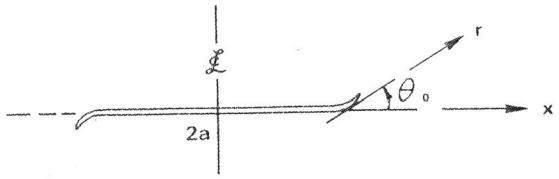

Figure 7 Angle of initial crack extension, θ_0

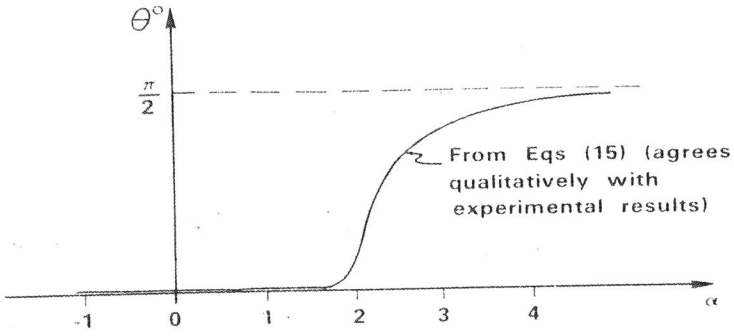

Figure 8 Variation of the angle of initial crack extension with biaxiality of loading

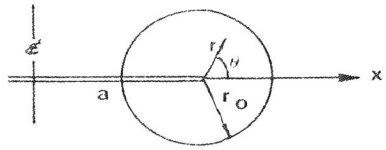

Figure 9 Local crack-tip region

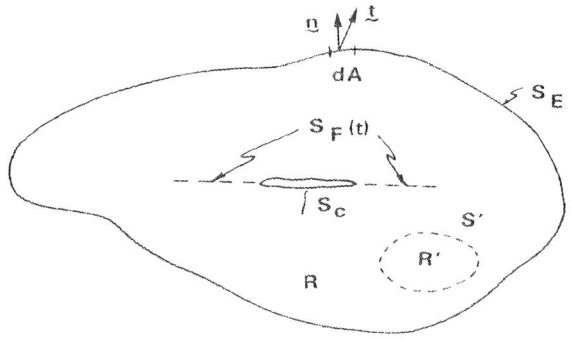

Figure 10 Crack propagating in a body

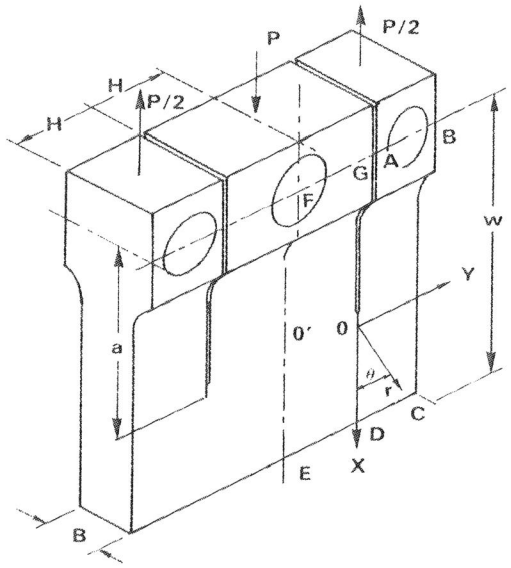

Figure 11 The compact shear specimen and associated coordinate system for mode II loading

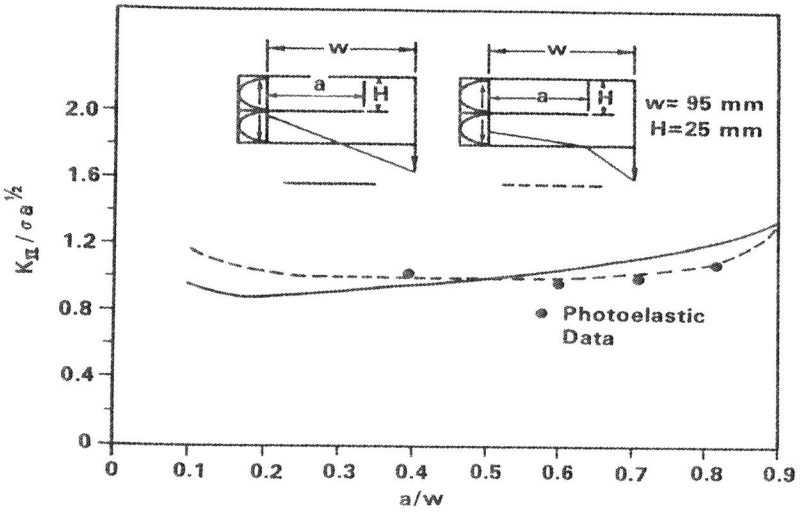

Figure 12 Comparison of effect of linear and bilinear stresses along specimen centerline on nondimensionalized stress intensity factor w = 95mm

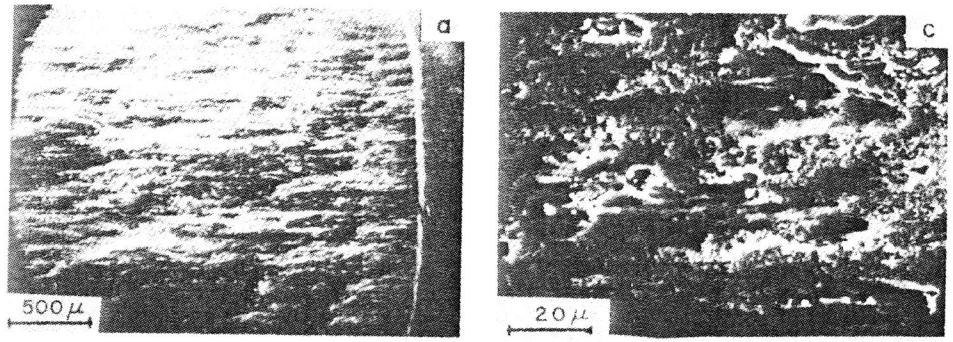

Figure 13 Typical scanning electron micrograph of a Mode II fracture surface of 2024-T4 aluminum